Inorganic Chemistry

Article

pubs.acs.org/IC

A Templated Method to Bi_2WO_6 Hollow Microspheres and Their Conversion to Double-Shell Bi_2O_3/Bi_2WO_6 Hollow Microspheres with Improved Photocatalytic Performance

Xiaona Li, Renkun Huang, Yanhua Hu, Yongjuan Chen, Wenjun Liu, Rusheng Yuan, and Zhaohui Li*

Research Institute of Photocatalysis, Fujian Provincial Key Laboratory of Photocatalysis, State Key Laboratory Breeding Base, Fuzhou University, Fuzhou 350002, People's Republic of China

Supporting Information

ABSTRACT: Bi_2WO_6 hollow microspheres with dimension of ca. 1.5 μm were synthesized via a hydrothermal method using polystyrene particles as the template. The as-prepared Bi_2WO_6 hollow microspheres can be further transformed to double-shell Bi_2O_3/Bi_2WO_6 hollow microspheres. The samples were fully characterized by X-ray diffraction, scanning electron microscopy, transmission electron microscopy (TEM), high-resolution TEM, N_2-sorption Brunauer–Emmett–Teller surface area, UV–vis diffuse-reflectance spectroscopy, and X-ray photoelectron spectroscopy. The as-formed double-shell Bi_2O_3/Bi_2WO_6 hollow microspheres exhibit enhanced photocatalytic activity due to the hollow nature and formation of the p–n junction between p-type Bi_2O_3 and n-type Bi_2WO_6. The study provides a general and effective method in the fabrication of composition and dimension-tunable composite hollow microspheres with sound heterojunctions that may show a variety of applications.

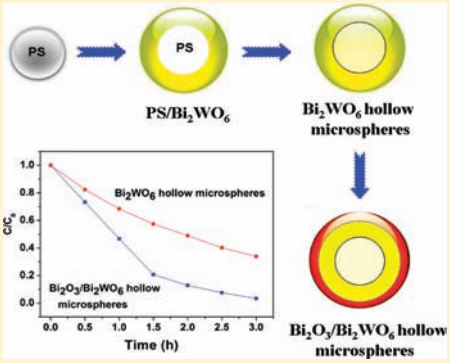

1. INTRODUCTION

Hollow micro/nanosized spheres have shown wide applications as heterogeneous catalysts, drug-delivery agents, photonic materials, battery materials, and so on because of their unique chemical and physical properties compared to their solid counterparts.[1,2] By far, the templated method is the most effective method in the preparation of hollow micro/nanosized spheres.[3] Template-based syntheses of hollow spheres rely on formation of the desired sphere component on a sacrificial template followed by removal of the template.[4] The advantage of template-based syntheses is that the shape and size of the cavity of the as-formed hollow spheres can be determined by the involved template.[5] A variety of templates, such as polymer latex spheres,[6] silica sol,[7] gas bubbles, microemulsion droplets, etc., have been introduced in the preparation of hollow sphere materials.[8,9] As a generally applied template, polystyrene (PS) particles exhibit many excellent characteristics such as simple preparation, ease for surface functionalization, and flexibility in size variation.[10,11] The use of PS particles as templates in the preparation of a variety of hollow spheres has already been demonstrated.[12,13] For example, conduction polymer polyaniline and polypyrrole hollow microspheres have been successfully prepared by oxidative polymerization of aniline or pyrrole on the surface of sulfonated PS followed by template removal by calcination.[14,15] ZnO–TiO_2 mixed metal oxide hierarchical hollow spheres have been fabricated by coating the functionalized PS template beads with successive layers of ZnO and TiO_2 nanoparticles, followed by calcination of the resulting PS/ZnO–TiO_2 core–shell composite particles at elevated temperature.[16]

Bi_2WO_6 is a promising visible-light-responsive photocatalyst for the degradation of organic pollutants and water splitting.[17,18] Nanoparticles, nanoplates, as well as some complicated 3D hierarchical structures of Bi_2WO_6 including flowerlike microspheres,[19] nestlike structure,[20] hollow microspheres, and octahedron-like assemblies have all been reported.[21,22] The photocatalytic performance of Bi_2WO_6 has been found to be greatly influenced by its morphology. Hollow spheres of Bi_2WO_6 show a superior photocatalytic performance because of a more efficient use of the light source via multiple reflections of light within the interior cavity.[23] Combining two or more semiconductors with appropriate band positions to improve the photocatalytic performance of the semiconductors is an established idea because it can lead to an enhanced charge separation and interfacial charge-transfer efficiency.[16,24] Especially, the fabrication of a p–n junction is believed to be the most effective because of the existence of an internal electric field.[25] Actually, coupling Bi_2WO_6 to another semiconductor has also been tried previously, and a couple of composite photocatalysts comprised of n-type Bi_2WO_6 and p-type Bi_2O_3 have already been fabricated, which show an improved photocatalytic performance.[26−29] However, to the best of our knowledge, the fabrication of hollow microspheres of a double-shell Bi_2O_3/Bi_2WO_6 composite, which can make an effective and sound p–n junction between p-type Bi_2O_3 and n-type Bi_2WO_6, has never been reported previously.

Received: February 29, 2012
Published: May 16, 2012

   dx.doi.org/10.1021/ic300454q | *Inorg. Chem.* 2012, 51, 6245–6250

Herein, we report the preparation of hollow microspheres of Bi_2WO_6 via a PS template method and their transformation to the double-shell Bi_2O_3/Bi_2WO_6 hollow microspheres by a hydrothermal treatment. This method is expected to be applied in the fabrication of hollow microsphere composite materials with a sound heterojunction. The combination of the hollow structure and the existence of the p−n junction in the as-prepared Bi_2O_3/Bi_2WO_6 composite render it with an improved photocatalytic performance under visible-light irradiation.

2. EXPERIMENTAL SECTION

Materials. Styrene (ST; Fluka) and acetoacetoxyethyl methacrylate (AAEM; 97%, Aldrich) were distilled under N_2. Sodium peroxydisulfate (SPDS; 97%), $Bi(NO_3)_3{\cdot}5H_2O$ (99.9%), Na_2WO_4, and NaOH were used as received without further purification.

Preparation of PS Particles. Functionalized PS particles with diameter of ca. 500 nm were prepared by the emulsion polymerization of ST and AAEM following a previously reported method.[30] A double-necked glass reactor equipped with a reflux condenser was purged with N_2. Deionized water (170 mL) and appropriate amounts of ST and AAEM were added into the reactor, and the reaction mixture was stirred for 10 min at room temperature. Then the temperature was raised to 70 °C, and an aqueous solution of SPDS (0.30 g in 10 mL of deionized water) was added into the reaction mixture to initiate the polymerization process. The reaction was allowed to proceed at 70 °C for another 24 h, and PS particles were obtained as a stable dispersion in water with ca. 15% solid content.

Preparation of Bi_2WO_6 Hollow Microspheres. $Bi(NO_3)_3{\cdot}5H_2O$ (2.426 g, 5 mmol) was dissolved in 40 mL of deionized water, and the solution was stirred vigorously. A dispersion of the as-prepared PS particles (4 g) was added to the $Bi(NO_3)_3$ suspension, and the reaction was sonicated for 40 min. Subsequently, $Na_2WO_4{\cdot}2H_2O$ (0.825 g) in 10 mL of deionized water was added slowly to the mixture, and the reaction mixture was sonicated for another 40 min. The resulting reaction mixture was transferred to a 100 mL Teflon-lined autoclave and was reacted at 180 °C for 48 h. After being cooled to room temperature, the sample was washed with deionized water several times and dried at 60 °C. Also, the product was calcined at 500 °C for 4 h to remove the PS template. The bulk Bi_2WO_6 (SSR) sample was prepared from Bi_2O_3 and WO_3 via a conventional solid-state reaction according to the literature.[31]

Preparation of Bi_2O_3/Bi_2WO_6 Hollow Microspheres. A desired amount of $Bi(NO_3)_3{\cdot}5H_2O$ was dissolved in 20 mL of ethylene glycol (EG) and 40 mL of thanol, and the resulting solution was sonicated until it became clear. The as-obtained Bi_2WO_6 hollow spheres (1 g) were added to the solution and stirred. After that, the mixture was transferred to a Teflon-lined autoclave, sealed, and heated at 150 °C for 24 h. After being cooled to room temperature, the product was collected by filtration, washed with deionized water, and dried at 60 °C. Finally, the precursor was calcined at 450 °C for 3 h.

Characterizations. Powder X-ray diffraction (XRD) patterns were collected using a Bruker D8 Advance X-ray diffractometer (Cu $K\alpha_1$ irradiation, λ = 1.5406 Å). X-ray photoelectron spectroscopy (XPS) measurements were performed on a PHI Quantum 2000 XPS system with a monochromatic Al K_α source and a charge neutralizer. All of the binding energies were referred to the C 1s peak at 284.8 eV of the surface adventitious carbon. The morphology of the sample was characterized by a field-emission scanning electron microscope (model JSM-6700F). The transmission electron microscopy (TEM) and high-resolution TEM (HRTEM) images were measured by a JEOL model JEM 2010 EX instrument at an accelerating voltage of 200 kV. The specific surface area of the samples was measured by N_2 sorption at 77 K on an ASAP 2020 instrument and calculated by the Brunauer−Emmett−Teller (BET) method. UV−vis absorption spectra (UV−vis diffuse-reflectance spectrometry, DRS) of the powders were obtained for the dry-pressed disk samples using a UV−vis spectrophotometer (Cary 500 Scan spectrophotometer, Varian). $BaSO_4$ was used as a reflectance standard in the UV−vis DRS experiment.

Photocatalytic Test. The photocatalytic activity of the as-prepared samples was evaluated by the degradation of RhB under visible-light irradiation. A 500-W tungsten−halogen lamp was positioned inside a cylindrical Pyrex vessel and surrounded by a circulating water jacket (Pyrex) to cool the lamp. A cutoff filter was placed outside the Pyrex jacket to completely remove all wavelengths less than 420 nm to ensure irradiation with visible light only. A total of 80 mg of Bi_2O_3, Bi_2WO_6 (SSR), Bi_2WO_6, and Bi_2O_3/Bi_2WO_6 hollow microspheres was added to 80 mL of a RhB solution (10^{-5} mol L^{-1}). Prior to irradiation, the suspensions were magnetically stirred in the dark for 4 h to ensure the establishment of an adsorption/desorption equilibrium. At given irradiation time intervals, 3 mL of the suspension was collected, centrifuged, and filtered through a Millipore filter to separate the photocatalyst. The degraded solutions were analyzed by a Varian Cary 500 Scan UV−vis spectrophotometer, and the absorption peak at 554 nm for RhB was monitored.

3. RESULTS AND DISCUSSION

PS particles were prepared by the copolymerization of ST and AAEM according to a reported method.[30] The scanning electron microscopy (SEM) image reveals that the as-prepared PS particles own smooth surfaces and the particles are nearly monodispersed in size with ca. 500 nm diameter (Figure 1a).

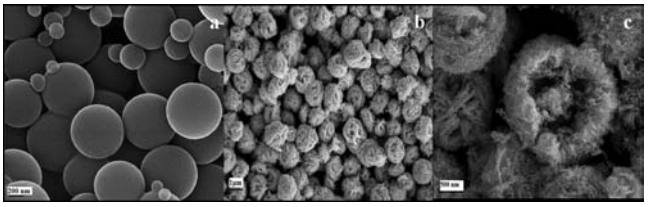

Figure 1. SEM images: (a) PS particles; (b) PS/Bi_2WO_6 composite microspheres; (c) Bi_2WO_6 hollow microspheres.

The added comonomer AAEM helps to stabilize the obtained colloidal system and renders the surface of the resulting PS particles with β-diketone functionality. For the formation of PS/Bi_2WO_6 core−shell composite particles, the first step is the adsorption of Bi^{3+} on the surface of PS, which can be facilely achieved because of the existence of the physical interaction between the surface β-diketone functionality and Bi^{3+} ions. In the next step, a Na_2WO_4 solution should be added slowly into the colloidal system to ensure its full reaction with the surface-adsorbed Bi^{3+}. An appropriate hydrothermal reaction temperature and reaction time is essential for the formation of well-defined core−shell PS/Bi_2WO_6 composite particles. Well-defined yarn-ball-like microspheres of PS/Bi_2WO_6 with dimension of about 1.5 μm can be obtained by heating the mixture at 180 °C for 48 h (Figure 1b). A lower hydrothermal temperature (160 °C) or a shorter reaction time (24 h) led to not well-formed microspheres, although the as-formed samples are also indexed to be orthorhombic Bi_2WO_6 (Figures S1 and S2 in the Supporting Information). To remove the interior PS core, the well-defined yarn-ball-like PS/Bi_2WO_6 microspheres were calcined at 500 °C and hollow yarn-ball-like microspheres with similar dimension were obtained, as evidenced from a broken microsphere shown in Figure 1c. Considering the size of the PS particles (500 nm), the resultant hollow microspheres should have a thick Bi_2WO_6 shell of about 500 nm. The thick Bi_2WO_6 shell is believed to provide enough mechanical support for these Bi_2WO_6 hollow microspheres after removal of the PS core. The XRD pattern of the sample shows 2θ peaks at 28.3°, 32.79°, 47.1°, 55.8°, 58.5°, 68.8°, 75.9°, and 78.4°, which correspond to the diffraction from the (131), (200), (202),

dx.doi.org/10.1021/ic300454q | Inorg. Chem. 2012, 51, 6245−6250

(331), (262), (400), (193), and (402) crystallographic planes of orthorhombic Bi_2WO_6 (JCPDS, No. 39-0256). This indicates that the shell of the microspheres is composed of pure orthorhombic Bi_2WO_6 (Figure 2a).

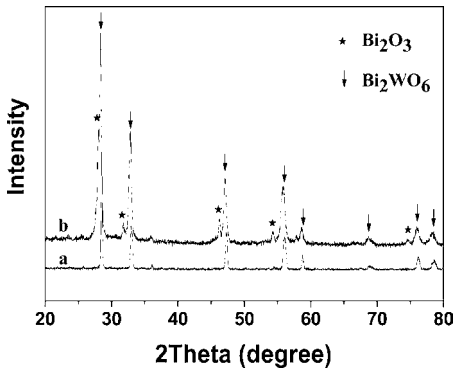

Figure 2. XRD patterns: (a) Bi_2WO_6 hollow microspheres; (b) Bi_2O_3/Bi_2WO_6 hollow microspheres.

To fabricate a Bi_2O_3/Bi_2WO_6 composite hollow microsphere, a thin layer of Bi_2O_3 was deposited over the as-formed Bi_2WO_6 hollow microspheres using $Bi(NO_3)_3$ as the Bi source and a mixture of EG and ethanol as the solvent. Strong coordinating solvent EG was chosen because it can react with the surface OH groups on the as-prepared Bi_2WO_6 microspheres by forming hydrogen bonds, and then the surface-adsorbed EG can further coordinate with Bi^{3+} to form a stable intermediate $Bi_2(OCH_2CH_2O)_3$. Hydrolysis of the intermediate $Bi_2(OCH_2CH_2O)_3$ followed by calcination at 450 °C led to the formation of Bi_2O_3 nanoparticles. Such a process can ensure the formation of a thin shell of Bi_2O_3 on the surface of Bi_2WO_6 hollow microspheres to make an effective and sound Bi_2O_3/Bi_2WO_6 p−n junction. The successful deposition of Bi_2O_3 on the surface of Bi_2WO_6 hollow microspheres was confirmed by the XRD pattern. In addition to the diffraction peaks assigned to orthorhombic Bi_2WO_6, the XRD pattern of the as-formed Bi_2O_3/Bi_2WO_6 composite shows 2θ peaks at 28.0°, 31.8°, 32.7°, 46.3°, 54.4°, and 74.7°, which correspond to (221), (002), (400), (402), (223), and (750) planes of tetragonal Bi_2O_3 (JCPDS, No. 01-074-1374; Figure 2b). The composite maintains its original morphology as microspheres except for the much smoother surface compared to the parent Bi_2WO_6 hollow microspheres (Figure 3a). The size of the composite

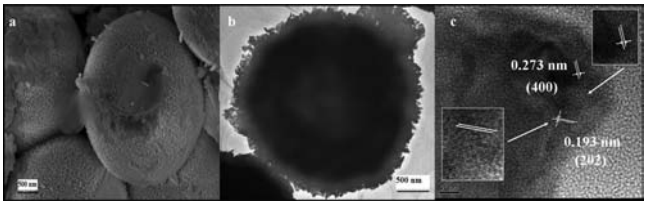

Figure 3. Images of Bi_2O_3/Bi_2WO_6 hollow microspheres: (a) SEM; (b) TEM; (c) HRTEM.

microspheres does not change obviously, indicating that the as-formed Bi_2O_3 shell is thin compared to the original Bi_2WO_6 shell. Theoretically, it is possible to tune the thickness of the Bi_2O_3 shell by changing the conditions during the Bi_2O_3 deposition process. To further obtain information about the structure of the sample, the as-prepared composite was characterized by TEM and HRTEM as well. In agreement with the SEM image, the TEM image of the composite shows that the microsphere has a dimension of about 1.5 μm, and the relatively pale center observed on the TEM image of a single microsphere further confirms that the as-prepared Bi_2WO_6/Bi_2O_3 microsphere has a hollow center (Figure 3b). The dimension of the cavity is estimated to be about 500 nm, comparable to the size of the template PS particles. The HRTEM image of the composite shows two types of intimately contacted lattice fringes, confirming formation of the junction between Bi_2WO_6 and Bi_2O_3 (Figure 3c). The lattice spacing of 0.273 nm corresponds to the interplanar distance between adjacent (400) crystallographic planes of Bi_2O_3, while the fringe of d = 0.193 nm matches that of the (202) plane of Bi_2WO_6.

XPS analyses were also carried out on the as-prepared Bi_2O_3/Bi_2WO_6 composite. The XPS spectrum in the W 4f region shows a binding energy at 34.7 eV for W $4f_{7/2}$ and at 36.8 eV for W $4f_{5/2}$, suggesting that W exists in the chemical state of W^{6+} (Figure 4a).[30] The high-resolution XPS spectra of the Bi $4f_{7/2}$ region can be deconvoluted into two peaks at around 158.8 and 160.1 eV and suggest that there are two types of Bi ions in the as-prepared Bi_2WO_6/Bi_2O_3 composite (Figure 4b). Considering that the binding energy of the Bi ion in pure Bi_2WO_6 exists in the range of 158−159 eV[19,20,28] and that for Bi_2O_3 in the range of 159−160 eV,[32] the peak at 158.8 eV can be ascribed to Bi^{3+} in Bi_2WO_6, while the other one at 160.1 eV originates from Bi^{3+} in Bi_2O_3. Because of the existence of several types of nonequivalent lattice O atoms, the XPS spectrum in the O 1s region is complicated and can be deconvoluted to three peaks at 533.8, 529.6, and 531.2 eV, which can be assigned to Bi−O in Bi_2O_3 and Bi−O and W−O in Bi_2WO_6 respectively (Figure 4c).[20,28]

The processes involved in the formation of Bi_2WO_6 hollow microspheres and their transformation to double-shell Bi_2O_3/Bi_2WO_6 composite hollow microspheres are summarized in Scheme 1. This provides an effective and general method for the fabrication of composite hollow microspheres with an effective and sound heterojunction that may show a variety of applications. An added advantage of this method is that the dimension of the hollow center, the thickness of the shell, and the ratio of the two constituents can be facilely adjusted by deliberately controlling the reaction conditions.

The as-prepared Bi_2WO_6 hollow microspheres show a BET surface area of 7.45 m^2 g^{-1}, which is about 30 times that prepared via the conventional solid-state reaction (0.28 m^2 g^{-1}). Bi_2O_3/Bi_2WO_6 hollow microspheres exhibit a BET specific surface area of 6.18 m^2 g^{-1}, comparable to that of the parent Bi_2WO_6 hollow microspheres. This indicates that the process during deposition of the Bi_2O_3 shell does not influence the BET specific surface area of Bi_2WO_6 hollow microspheres.

The UV−vis DRS spectra of the as-prepared Bi_2WO_6 hollow microspheres, Bi_2O_3/Bi_2WO_6, pure Bi_2O_3, and a mechanical mixture of Bi_2WO_6 and Bi_2O_3 with 5 wt % Bi_2O_3 are shown in Figure 5. The absorption edges of pure Bi_2O_3 and Bi_2WO_6 are determined to be 443 and 425 nm, respectively, corresponding to band gaps of 2.8 and 2.9 eV. These values are comparable to those reported in the literature.[28,33] The absorption edge of a mechanical mixture of Bi_2WO_6 and Bi_2O_3 is determined to be 434 nm, the value of which lies between those of pure Bi_2O_3 and Bi_2WO_6. However, to our surprise, the Bi_2O_3/Bi_2WO_6 composite hollow microspheres show an additional transition, with the absorption edge extending to 495 nm. We believe that a partial interfacial charge transfer between p-type Bi_2O_3 and n-

dx.doi.org/10.1021/ic300454q | Inorg. Chem. 2012, 51, 6245−6250

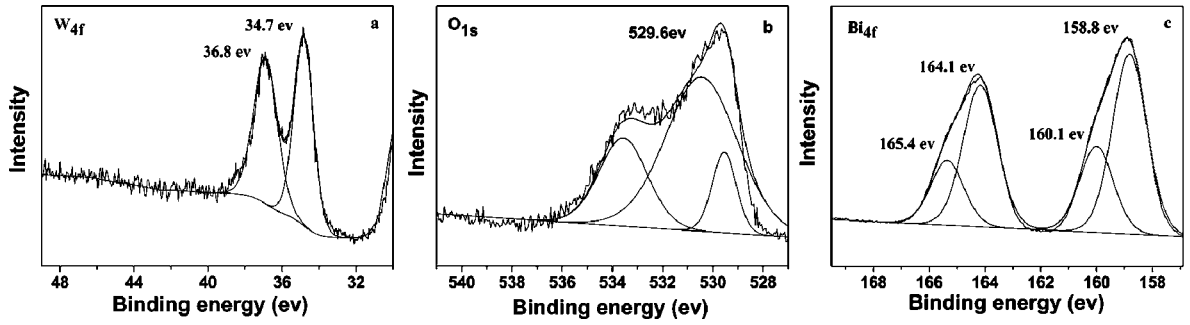

Figure 4. High-resolution XPS spectra of Bi_2O_3/Bi_2WO_6 hollow microspheres: (a) W 4f; (b) O 1s; (c) Bi 4f.

Scheme 1. Processes Involved in the Formation of Bi_2WO_6 Hollow Microspheres and Their Transformation to Double-Shell Bi_2O_3/Bi_2WO_6 Composite Hollow Microspheres

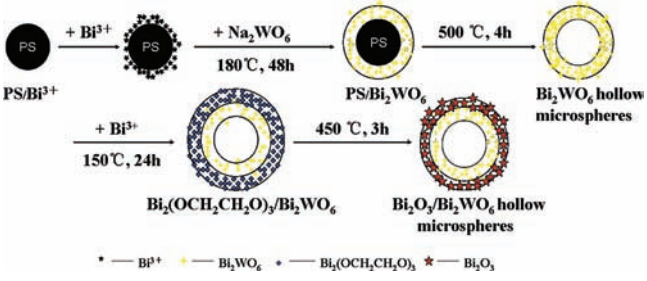

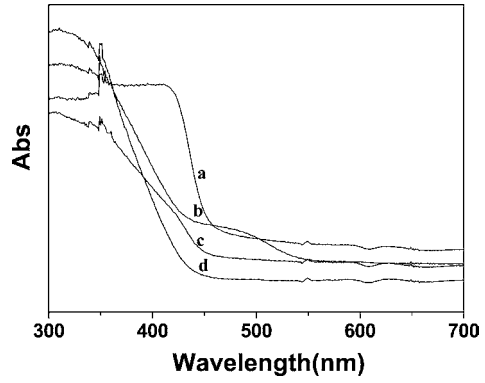

Figure 5. UV–vis DRS spectra: (a) Bi_2O_3; (b) Bi_2O_3/Bi_2WO_6 hollow microspheres; (c) mechanical mixture of Bi_2WO_6 and Bi_2O_3; (d) Bi_2WO_6 hollow microspheres.

type Bi_2WO_6 is probably responsible for this absorption because such a transition cannot be assigned to either Bi_2O_3 or Bi_2WO_6.

The photocatalytic performance of the samples was evaluated by decomposing a RhB aqueous solution under visible-light irradiation, and the results are shown in Figure 6. It is observed that Bi_2O_3 was almost photocatalytic inactive and only 8% of RhB was converted in 3 h over Bi_2WO_6 prepared via a solid-state reaction. On the contrary, 68% of RhB was converted over irradiated Bi_2WO_6 hollow microspheres in 3 h. Moreover, the incorporation of p-type Bi_2O_3 into n-type Bi_2WO_6 led to an obviously enhanced photocatalytic activity, and an almost complete degradation of RhB occurred within 3 h of irradiation. The improved performance observed over the Bi_2O_3/Bi_2WO_6 composite compared to Bi_2WO_6 hollow microspheres can be ascribed to formation of the p–n junction. Scheme 2a shows the energy-band schematic diagram for p-type Bi_2O_3 (E_{CB} = 0.33 V and E_{VB} = 3.13 V versus NHE) and n-type Bi_2WO_6 (E_{CB}

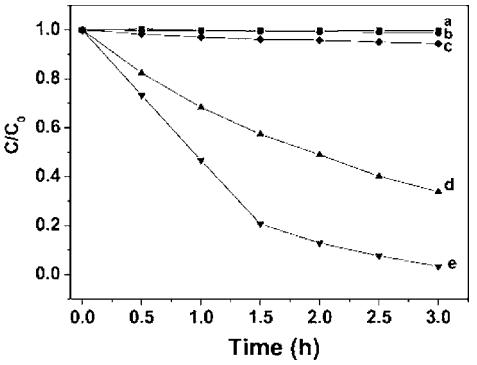

Figure 6. Temporal changes of the RhB concentration as monitored by the UV–vis absorption spectra at 554 nm under visible-light irradiation: (a) no catalyst; (b) Bi_2O_3; (c) Bi_2WO_6 (SSR); (d) Bi_2WO_6 hollow microspheres; (e) Bi_2O_3/Bi_2WO_6 hollow microspheres.

Scheme 2. Schematic Diagram of Charge Transfer between n-Type Bi_2WO_6 and p-Type Bi_2O_3: (A) before Contact; (B) after Formation of the p–n Junction

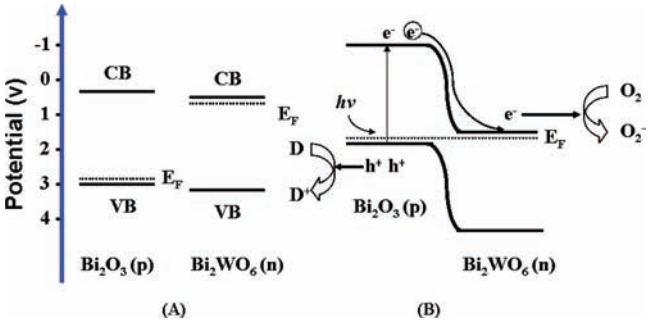

= 0.36 V and E_{VB} = 3.26 V versus NHE). When p-type Bi_2O_3 and n-type Bi_2WO_6 are contacted, the Fermi level of p-type Bi_2O_3 moves up, while in the meantime, that of n-type Bi_2WO_6 moves down until the equilibrium state is formed. Consistent with the moving of the Fermi level, the whole energy band of p-type Bi_2O_3 is raised up, while that of n-type Bi_2WO_6 is descended (Scheme 2b). An inner electric field from n-type Bi_2WO_6 to p-type Bi_2O_3 is thus established. Under visible-light irradiation, both Bi_2O_3 and Bi_2WO_6 can be excited to generate electron–hole pairs.[34] According to the energy-band schematic diagram shown in Scheme 2b, the photogenerated electrons on the conduction band of p-type Bi_2O_3 can transfer to that of n-type Bi_2WO_6, while simultaneously photogenerated holes can migrate from the valence band of n-type Bi_2WO_6 to that of p-type Bi_2O_3. Such migrations of the photogenerated carriers can be promoted by the internally formed electric field. Thus, the

dx.doi.org/10.1021/ic300454q | Inorg. Chem. 2012, 51, 6245–6250

photogenerated electrons and holes can be separated effectively because of formation of the p−n junction between p-type Bi_2O_3 and n-type Bi_2WO_6 interfaces. The separated photogenerated electrons and holes are then free to initiate reactions with the reactants adsorbed on the photocatalyst surface, leading to an enhanced photocatalytic activity.[35]

The hollow nature of the as-prepared Bi_2O_3/Bi_2WO_6 hollow microspheres is also responsible for its superior photocatalytic performance. The improvement of the catalytic activity due to the existence of the hollow morphology has been previously reported.[36] Especially in photocatalysis, such a hollow structure can also allow multiple reflections of UV−vis light within the hollow center, which can make more efficient use of the light source.[37] Moreover, photocatalysts in microsphere morphology can be more readily separated from the slurry system by filtration after the photocatalytic reaction and reused than the nanosized samples because of their large weight, weak Brownian motion, and good mobility.[38] All of these make the photocatalysts with hollow microsphere morphology appealing photocatalysts in the aqueous photocatalytic reaction.

4. CONCLUSION

In summary, a templated method has been used to synthesize Bi_2WO_6 hollow microspheres, which can be further converted to double-shell Bi_2O_3/Bi_2WO_6 hollow microspheres. The as-formed Bi_2O_3/Bi_2WO_6 hollow microspheres exhibit obviously enhanced photocatalytic activity because of its hollow center and the existence of the p−n junction between p-type Bi_2O_3 and n-type Bi_2WO_6. The study provides a general and effective method in the fabrication of composition and dimension-tunable composite hollow microspheres with a sound heterojunction that may show a variety of applications.

■ ASSOCIATED CONTENT

Ⓢ Supporting Information

SEM images and XRD patterns of PS/Bi_2WO_6 composite microspheres synthesized under different reaction conditions. This material is available free of charge via the Internet at http://pubs.acs.org.

■ AUTHOR INFORMATION

Corresponding Author

*E-mail: zhaohuili1969@yahoo.com. Tel: 86-591-83779260.

Notes

The authors declare no competing financial interest.

■ ACKNOWLEDGMENTS

The work was supported by the National Natural Science Foundation of China (Grants 20977016 and U1033603), National Basic Research Program of China (973 Program 2011CB612314), and Program for Changjiang Scholars and Innovative Research Team in University (Program PCSIRT0818). The Award Program for Minjiang Scholar Professorship and the NSF for Fujian Province for Distinguished Young Investigator Grant 2009J06004 to Z.L. are also acknowledged.

■ REFERENCES

(1) Li, X. X.; Xiong, Y. J.; Li, Z. Q.; Xie, Y. *Inorg. Chem.* **2006**, *45*, 3493−3495.
(2) Zhu, H. T.; Wang, J. X.; Wu, D. X. *Inorg. Chem.* **2009**, *48*, 7099−7104.
(3) Zhang, D. F.; Zhang, H.; Shang, Y.; Guo, L. *Cryst. Growth Des.* **2011**, *11*, 3748−3753.
(4) Strandwitz, N. C.; Stucky, G. D. *Chem. Mater.* **2009**, *21*, 4577−4582.
(5) Jia, G.; You, H. P.; Song, Y. H.; Huang, Y. J.; Yang, M.; Zhang, H. J. *Inorg. Chem.* **2010**, *49*, 7721−7725.
(6) Su, Y.; Yan, R.; Dan, M. H.; Xu, J. X.; Wang, D.; Zhang, W. Q.; Liu, S. G. *Langmuir* **2011**, *27*, 8983−8989.
(7) Tong, S. T.; Mao, L.; Zhang, X. H.; Jia, C. Q. *Ind. Eng. Chem. Res.* **2011**, *50*, 13825−13830.
(8) Mazur, M. *J. Phys. Chem. C* **2008**, *112*, 13528−13534.
(9) Carroll, N. J.; Pylypenko, S.; Atanassov, P. B.; Petsev, D. N. *Langmuir* **2009**, *25*, 13540−13544.
(10) Shi, W.; Sahoo, Y.; Swihart, M. T.; Prasad, P. N. *Langmuir* **2005**, *21*, 1610−1617.
(11) Li, H. Q.; Ha, C. S.; Kim, I. *Langmuir* **2008**, *24*, 10552−10556.
(12) Duan, G. T.; Lv, F. J.; Cai, W. P.; Luo, Y. Y.; Li, Y.; Liu, G. Q. *Langmuir* **2010**, *26*, 6295−6302.
(13) Deng, Z. W.; Chen, M.; Gu, G. X.; Wu, L. M. *J. Phys. Chem. B* **2008**, *112*, 16−22.
(14) Park, M. K.; Onishi, K.; Locklin, J.; Caruso, F.; Advincula, R. C. *Langmuir* **2003**, *19*, 8550−8554.
(15) Fujii, S.; Matsuzawa, S.; Nakamura, Y.; Ohtaka, A.; Teratani, T.; Akamatsu, K.; Tsuruoka, T.; Nawafune, H. *Langmuir* **2010**, *26*, 6230−6239.
(16) Agrawal, M.; Gupta, S.; Pich, A.; Zafeiropoulos, N. E.; Stamm, M. *Chem. Mater.* **2009**, *21*, 5343−5348.
(17) Shang, M.; Wang, W. Z.; Sun, S. M.; Zhou, L.; Zhang, L. *J. Phys. Chem. C* **2008**, *112*, 10407−10411.
(18) Shi, R.; Huang, G.; Lin, J.; Zhu, Y. F. *J. Phys. Chem. C* **2009**, *113*, 19633−19638.
(19) Liu, S. W.; Yu, J. G. *J. Solid State Chem.* **2008**, *181*, 1048−1055.
(20) Wu, J.; Duan, F.; Zheng, Y.; Xie, Y. *J. Phys. Chem. C* **2007**, *111*, 12866−12871.
(21) Li, Y. Y.; Liu, J. P.; Huang, X. T.; Li, G. Y. *Cryst. Growth Des.* **2007**, *7*, 1350−1355.
(22) Li, Y. Y.; Liu, J. P.; Huang, X. T. *Nano Lett.* **2008**, *3*, 365−371.
(23) Ma, D.; Huang, S. M.; Chen, W. X.; Hu, S. W.; Shi, F. F.; Fan, K. *J. Phys. Chem. C* **2009**, *113*, 4369−4374.
(24) Lv, K.; Li, J.; Qing, X. X.; Li, W. Z.; Chen, Q. Y. *J. Hazard. Mater.* **2011**, *189*, 329−335.
(25) Nikoobakht, B.; Bonevich, J.; Herzing, A. *J. Phys. Chem. C* **2011**, *115*, 9961−9969.
(26) Shang, M.; Wang, W. Z.; Zhang, L.; Sun, S. M.; Wang, L.; Zhou, L. *J. Phys. Chem. C* **2009**, *113*, 14727−14731.
(27) Xiao, Q.; Zhang, J.; Xiao, C.; Tan, X. K. *Catal. Commun.* **2008**, *9*, 1247−1253.
(28) Gui, M. S.; Zhang, W. D.; Su, Q. X.; Chen, C. H. *J. Solid State Chem.* **2011**, *184*, 1977−1982.
(29) Ge, M.; Li, Y. F.; Liu, L.; Zhou, Z.; Chen, W. *J. Phys. Chem. C* **2011**, *115*, 5220−5225.
(30) Agrawal, M.; Pich, A.; Zafeiropoulos, N. E.; Gupta, S.; Pionteck, J.; Simon, F.; Stamm, M. *Chem. Mater.* **2007**, *19*, 1845−1852.
(31) Zhang, S. C.; Zhang, C.; Man, Y.; Zhu, Y. F. *J. Solid State Chem.* **2006**, *179*, 62−69.
(32) Moulder, J. F.; Stickle, W. F.; Sobol, P. E.; Bomben, K. D. *Handbook of X-ray Photoelectron Spectroscopy*; Physical Electronics, Inc.: Chanhassen, MN, 1995.
(33) Bian, Z. F.; Zhu, J.; Wang, S. H.; Cao, Y.; Qian, X. F.; Li, H. X. *J. Phys. Chem. C* **2008**, *112*, 6258−6262.
(34) Dai, G. P.; Yu, J. G.; Liu, G. *J. Phys. Chem. C* **2011**, *115*, 7339−7346.
(35) Guan, M. L.; Ma, D. K.; Hu, S. W.; Chen, Y. J.; Huang, S. M. *Inorg. Chem.* **2011**, *50*, 800−805.
(36) Mandal, S.; Sathish, M.; Saravanan, G.; Datta, K. K. R.; Ji, Q. M.; Hill, J. P.; Abe, H.; Honma, I.; Ariga, K. *J. Am. Chem. Soc.* **2010**, *132*, 14415−14417.
(37) Yu, J. G.; Yu, X. X. *Environ. Sci. Technol.* **2008**, *42*, 4902−4907.

(38) Yu, J. G.; Yu, X. X.; Huang, B. B.; Zhang, X. Y.; Dai, Y. *Cryst. Growth Des.* **2009**, *9*, 1474−1480.